THE JOURNAL OF PHYSICAL CHEMISTRY LETTERS
A JOURNAL OF THE AMERICAN CHEMICAL SOCIETY

pubs.acs.org/JPCL

Letter

Colloidal Nanoribbons: From Infrared to Visible

Zhoufeng Jiang,[‖] Yiteng Tang,[‖] Antara Debnath Antu, Shashini M. Premathilaka, Marilyn Louise Cayer, Carol A. Heckman, Pavel Moroz, Mikhail Zamkov, and Liangfeng Sun*

Cite This: *J. Phys. Chem. Lett.* 2022, 13, 8987−8992

Read Online

ACCESS | Metrics & More | Article Recommendations | Supporting Information

ABSTRACT: Using the cation-exchange method, colloidal PbS nanoribbons are converted completely into CdS nanoribbons. This process expands the emission spectrum of the nanoribbons from infrared to visible. The morphology of nanoribbons remains the same after cation exchange, but the crystal structure changes from rock salt to zincblende. CdS nanoribbons exhibit blue band-edge photoluminescence under ultraviolet-light excitation. Cathodoluminescence spectroscopy of the CdS nanoribbons shows multicolor (blue, green, and red) emissions. Further time-resolved photoluminescence spectroscopy studies show that the lifetime of the midgap states is more than 2 orders of magnitude longer than that of the band-edge states.

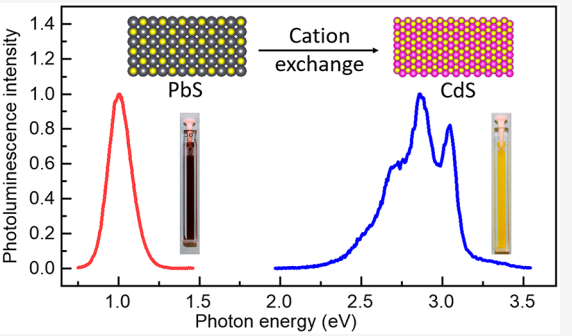

In the past decade, colloidal nanoplatelets (also known as quantum belts[1,2] or quantum disks[3,4]) made of CdX (X = S, Se, or Te) have been developed and demonstrated superior optical properties, including high photoluminescence quantum yields,[5−7] short radiative lifetimes,[4,8] and low lasing thresholds.[9−14] The infrared counterpart of this bright visible emitter, colloidal PbS nanosheets, has also been synthesized,[15−20] demonstrating a highly efficient carrier multiplication,[21] large charge-carrier mobilities,[22,23] and unique topological properties.[24] Robust synthetic methods have been developed[19] to synthesize PbS nanosheets with tunable thickness[25] and lateral size.[26,27] Converting the well-defined two-dimensional PbS into CdS can bridge the infrared and visible spectra aiming at optoelectronic and photonic devices exhibiting a broad energy spectrum.

In this work, we convert colloidal PbS nanoribbons to CdS nanoribbons by using the cation-exchange method.[28−31] The morphology of the nanoribbons remains the same, but their optical properties change significantly. We use both cathodoluminescence and photoluminescence (static and time-resolved) spectroscopies to study the emission states of the nanoribbons. The cathodoluminescence shows blue, green, and red emissions, revealing all emission states in the visible spectrum. The band-edge states of CdS nanoribbons emit light at a rate one order of magnitude faster than that of PbS nanoribbons, but the light emission from the midgap states of CdS nanoribbons is much slower.

We synthesized colloidal PbS nanoribbons using organometallic precursors following our method developed previously (section A of the Supporting Information).[20] Chloroalkane was added as the co-solvent to trigger two-dimensional attachment to form nanoribbons. The synthesized PbS nanoribbons were then dispersed in 1-octadecene and injected into the Cd oleate solution at 160 °C for cation exchange. The reaction was stopped after the solution turned yellow (section B of the Supporting Information). During the cation-exchange reaction, the Pb cations are replaced by Cd cations. This is typically a self-limiting process resulting in a core/shell heterogeneous structure.[30−32] However, we achieved a complete cation exchange at 160 °C and obtained pure CdS nanoribbons instead of PbS/CdS core/shell nanoribbons.[33]

After cation exchange, the morphology of the nanoribbons remains the same, but the crystal structure changes significantly. The transmission electron microscopy (TEM) image (Figure 1a) shows the original PbS nanoribbons have an average width of 20 nm and a length of >50 nm (Figure 1a). After cation exchange, the width and length of the nanoribbons remain the same (Figure 1b). The Pb cations in PbS nanoribbons are completely replaced by Cd cations, as evidenced by energy-dispersive X-ray spectroscopy (EDX) measurements (section C of the Supporting Information). Moire patterns appear in the overlapping areas of both PbS and CdS nanoribbons, indicating good crystallinity. The selected area electron diffraction (SAED) image shows a square pattern from PbS nanoribbons (Figure 1a, bottom left corner inset) but a hexagonal pattern from CdS nanoribbons (Figure 1b, bottom left corner inset). The square pattern reveals that the top and bottom surfaces of the nanoribbon are

Received: August 1, 2022
Accepted: September 20, 2022
Published: September 23, 2022

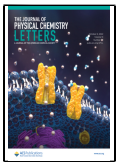

https://doi.org/10.1021/acs.jpclett.2c02390
J. Phys. Chem. Lett. 2022, 13, 8987−8992

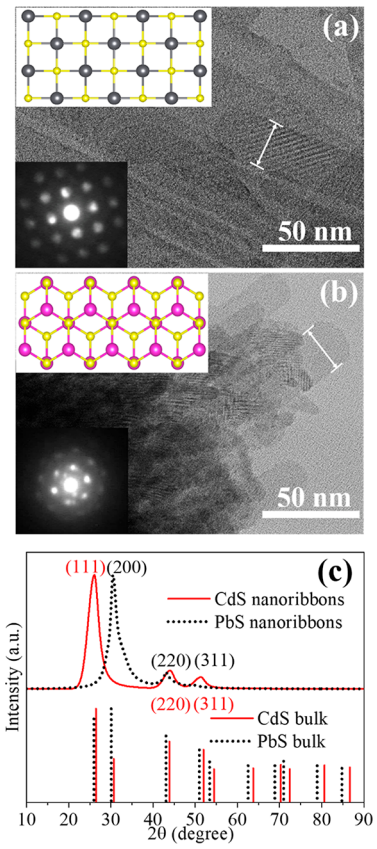

Figure 1. TEM images of (a) PbS and (b) CdS nanoribbons. The SAED pattern is shown in the bottom left corner of each image, which matches the (100) and (111) planes (top left corner) of PbS and CdS, respectively. Legend: Pb atom, gray sphere; Cd atom, pink sphere; S atom, yellow sphere. (c) X-ray diffraction patterns of PbS (dotted line) and CdS (solid line) nanoribbons. The standard diffraction patterns (vertical lines) of galena (PbS bulk) and hawleyite (CdS bulk) powders are shown as references. For CdS nanoribbons, three diffraction peaks at 26.5°, 44.0°, and 52.1° are identified, corresponding to the (111), (220), and (311) planes, respectively, of hawleyite CdS. For PbS nanoribbons, two diffraction peaks at 30.5° and 43.1° are identified, corresponding to the (200) and (220) planes, respectively, of the cubic PbS crystal. The diffraction peak of the (311) plane from the PbS nanoribbons is barely observable.

{100} facets of the rock-salt crystal structure of PbS, which is the same as that of PbS nanosheets.[33] However, the hexagonal diffraction pattern of CdS nanoribbons indicates that the basal plane is likely the {111} plane of zincblende CdS.

Further characterization of the nanoribbons using X-ray diffraction (XRD) confirms the change in crystal structure as well as the crystal basal plane. The XRD pattern of PbS nanoribbons shows the (200) and (220) diffraction peaks of galena (rock-salt structure). The diffraction pattern of CdS nanoribbons matches that of the (111), (220), and (311) planes of hawleyite CdS (zincblende structure). Because the zincblende structure is more stable than the rock-salt structure of CdS,[34] the transition of the crystal structure is expected during the cation-exchange process.

In contrast to PbS quantum dots (section D of the Supporting Information), the (111) diffraction peak from PbS nanoribbons is absent while the (200) peak dominates in the diffraction pattern (Figure 1c). It is because the basal plane of the nanoribbon is the crystal (100) plane,[33] which faces up when the nanoribbons are deposited on the substrate. The edge facet of the PbS nanoribbon belongs to the (110) plane. Some nanoribbons may "stand" with their edges on the substrate, showing the (220) peak. The nanoribbon has no {111} facet,[20] which explains the absence of the (111) peak in the XRD data.

As opposed to PbS nanoribbons, CdS nanoribbons show a dominant (111) diffraction peak together with small (220) and (311) peaks. This result is consistent with the hexagonal SAED pattern (Figure 1b, bottom left corner inset), confirming the basal plane of CdS nanoribbons is the {111} plane. Interestingly, the hexagonal basal plane of the (111) facet occurs in colloidal CdS nanoribbons obtained by thermal decomposition[35] and in the PbS/CdS core/shell nanoribbons obtained using the cation-exchange method.[16]

The optical properties of the nanoribbons change significantly after cation exchange. The color of the nanoribbon solution turns from dark brown (Figure 2a, inset) to vivid

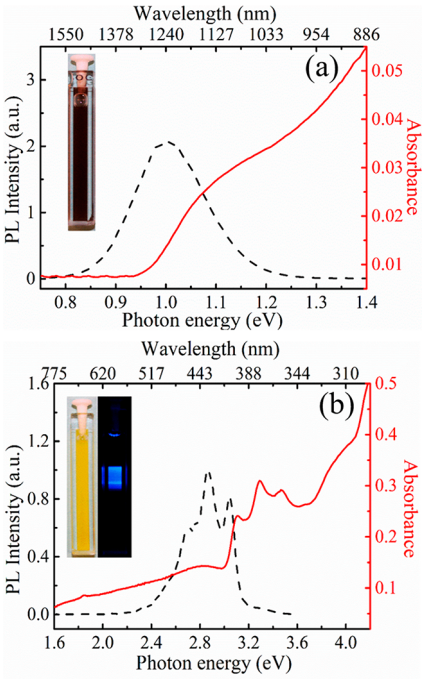

Figure 2. (a) Photoluminescence (PL) (dashed line) and optical absorption (solid line) spectra of PbS nanoribbons. The inset is a photograph of the PbS nanoribbon solution in a cuvette. (b) Photoluminescence (dashed line) and optical absorption (solid line) spectra of CdS nanoribbons. The inset shows photographs of the CdS nanoribbon solution in the room light (left) and under ultraviolet excitation (337 nm) in the dark (right).

yellow (Figure 2b, left inset), indicating the change in the energy gap. As-synthesized CdS nanoribbons exhibited a low photoluminescence intensity. We suspect that cation exchange creates defects in the crystal that quenches the photoluminescence. We anneal the nanoribbons in solution at 100 °C for 12 h (section E of the Supporting Information) to reduce the defects. The XRD measurements demonstrate that thermal annealing does not change the crystal structure (section F of the Supporting Information) but improves the photoluminescence efficiency significantly. In the optical absorption spectrum, the annealed nanoribbons show sharp optical absorption peaks that do not exist in the nanoribbons before annealing (section E of the Supporting Information). The improvement of optical properties is likely due to the

https://doi.org/10.1021/acs.jpclett.2c02390
J. Phys. Chem. Lett. 2022, 13, 8987−8992

reduction of defect states, as demonstrated in the CdSe/CdS dot/rod system.[36]

Under ultraviolet-laser excitation, the CdS nanoribbons emit blue light while the PbS nanoribbons emit infrared light. The optical absorption and photoluminescence spectra of the PbS nanoribbons demonstrate an optical bandgap of ∼1.0 eV (Figure 2a). The optical absorption and emission of CdS nanoribbons are mainly in the ultraviolet and visible spectra, where multiple peaks appear (Figure 2b). The optical absorption peaks are at 3.1, 3.3, and 3.5 eV, while the photoluminescence peaks are at 2.7, 2.9, and 3.0 eV. The photoluminescence quantum yield of the as-synthesized PbS nanoribbons is a few percent. It can be improved to >30% after surface passivation.[20] Upon excitation at 377 nm, the CdS nanoribbons have a photoluminescence (violet to blue) quantum yield of ∼3.7%. It is higher than the quantum yield (2%) of CdS nanoplatelets reported by Diroll et al.[37] If they are excited at 445 nm, the photoluminescence (green to red) quantum yield reaches ∼15%.

Both CdS and PbS nanoribbons have thickness-dependent energy gaps owing to quantum confinement (Figure 3). With

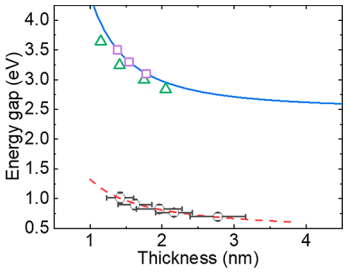

Figure 3. Thickness-dependent energy gap of CdS (solid line) and PbS (dashed line) nanoribbons. The dashed line represents the fitting curve for the experimental data (circles).[20] The solid line represents the calculated results based on eq 1. The experimental data for CdS nanoplatelets obtained by Ithurria et al.[8] are indicated by triangles. The results for the CdS nanoribbons are indicated by squares.

the quantum-confinement model, we can estimate the thickness of the nanoribbon from the energy of the emitted photon. The energy of a photon emitted from an infinite quantum well of width L is[4,5]

$$\hbar\omega_{\upsilon} = E_{\mathrm{g}}(\mathrm{bulk}) + \frac{h^2}{8L^2}\left(\frac{1}{m_{\mathrm{e}}} + \frac{1}{m_{\mathrm{h}}}\right) \quad (1)$$

For CdS, the bandgap of the bulk E_{g}(bulk) is 2.5 eV.[4] The effective masses of the electron (m_{e}) and the hole (m_{h}) are $0.205m_0$ and $5m_0$, respectively (m_0 is the mass of an electron).[4] On the basis of eq 1, the thickness corresponding to the absorption peak at 3.3 eV (Figure 2b) is calculated to be 1.53 nm, which is ∼4.5 monolayers of the atoms in the ⟨111⟩ direction of the CdS crystal. The two side peaks in the absorption spectrum are at 3.1 and 3.5 eV. The energy difference between the neighboring peaks (0.2 eV) is much larger than the energy difference between the electron to light-hole and the electron to heavy-hole transitions (<0.1 eV).[8] Therefore, multiple absorption peaks are not due to the difference in the hole mass, but the difference in the thickness. Using eq 1, we find the thickness corresponding to the peak of 3.1 eV is 1.36 nm (4 monolayers) and the peak of 3.5 eV is 1.7 nm (5 monolayers).

The thickness-dependent energy gap of PbS nanoribbons follows the semiempirical equation derived from the literature data[20]

$$E_{\mathrm{gap}}(L) = E_{\mathrm{gap}}(\infty) + \frac{1}{1.48L - 0.43} \quad (2)$$

The bulk PbS has an $E_{\mathrm{gap}}(\infty)$ of 0.41 eV. On the basis of this equation, we find the thickness corresponding to the 1.0 eV energy gap is 1.4 nm. It is close to the central thickness (1.53 nm) of the CdS nanoribbons obtained through cation exchange. It is expected because the cation exchange preserves the thickness.

The spectral features of CdS nanoribbons are different from those of PbS nanoribbons. The optical absorption and photoluminescence spectra of CdS nanoribbons reveal three peaks. The photoluminescence from the PbS nanoribbons shows only one peak. The exciton peak in the optical absorption spectrum is broad and blended with the band continuum. The difference is likely due to the different thickness-dependent confinement energy in these two different materials. The energy-gap difference between the neighbor exciton peaks from CdS nanoribbons is ∼0.2 eV. For the PbS nanoribbons with thicknesses of ∼1.4 nm, the average energy-gap difference between the neighbor thicknesses (e.g., 5 monolayers and 4.5 monolayers) is ∼0.09 eV based on eq 2. This small energy difference is "smeared out" by homogeneous and inhomogeneous broadenings in the spectra. Therefore, only one peak is observed in either the photoluminescence or the optical absorption spectrum of the PbS nanoribbons. However, the large energy-gap difference between the neighbor thicknesses in CdS nanoribbons makes each peak observable in the photoluminescence and the optical absorption spectra (Figure 2).

In addition to the difference in the optical spectra, the difference in the photoluminescence lifetime is also remarkable. The photoluminescence e-folding lifetime of CdS nanoribbons is 1.6 ns. It is 40 times shorter than the PbS nanoribbons (64 ns) (section G of the Supporting Information). Compared with the microsecond lifetime of PbS quantum dots,[38] the lifetimes of the PbS nanosheets[16,33] and nanoribbons[20] are short. The CdS nanoribbon's lifetime is even shorter. In contrast to the quantum dots made of the same material, CdS (∼20 ns),[4] the CdS nanoribbon's lifetime is still one order of magnitude shorter. Other colloidal two-dimensional nanostructures (including CdSe nanoplatelets,[8,39] CdS, and CdSe quantum disks[4]) also exhibit fast photoluminescence decays. This could be attributed to the enhanced exciton oscillator strength in the two-dimensional structure,[8,40] formation of "free excitons",[4] or mixing between bright and dark exciton states.[4]

There is still a significant absorbance (Figure 2b) below 3.1 eV (the lowest-energy exciton peak of CdS nanoribbons), which is likely due to the contribution from midgap states. In contrast, the original PbS nanoribbons do not show significant optical absorption below the bandgap (Figure 2a), indicating the midgap states are negligible. When the PbS nanoribbons are excited with a sub-bandgap light (∼1300 nm), no photoluminescence is detected. However, the midgap states in CdS nanoribbons are emissive. When CdS nanoribbons are excited below the bandgap (445 nm), the emission spectrum shows a broad photoluminescence peak extending beyond 600 nm into the near-infrared region (Figure 4, inset b). Interestingly, CdS quantum dots also exhibit a photo-

https://doi.org/10.1021/acs.jpclett.2c02390
J. Phys. Chem. Lett. 2022, 13, 8987−8992

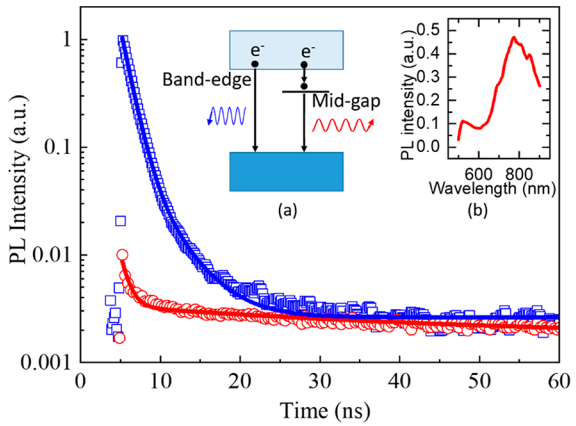

Figure 4. Photoluminescence (PL) decay traces of band-edge states (squares) and midgap states (circles) of CdS nanoribbons excited at 400 nm and measured at 435 and 720 nm, respectively. The solid lines passing through the data points are the fitting curves. Inset a is a diagram showing the band-edge state and midgap state and the electron transitions. Inset b shows the photoluminescence spectrum of CdS nanoribbons excited at 445 nm.

luminescence peak at ~770 nm.[41] The red emission is attributed to sulfur vacancies in a bulk CdS.[42] It also explains the sub-bandgap emission from the CdS quantum dots.[43−45] Further studies with time-resolved photoluminescence spectroscopy reveal that the exciton dynamics in the midgap states are very different from those of the band-edge states.

The photoluminescence from CdS nanoribbons demonstrates two distinguished decay dynamics (Figure 4). One is fast with a lifetime (τ_1) of ~1 ns, and the other is slow with a lifetime (τ_2) of ~10^2 ns (Table 1). Both blue (435 nm) and

Table 1. Results of the Analysis of the Time-Resolved Photoluminescence[a]

emitting state	A_1	τ_1 (ns)	f_1 (%)	A_2	τ_2 (ns)	f_2 (%)
band-edge	62.15	1.27	89	0.04	256	11
midgap	0.613	1.84	2	0.274	268	98

[a] A_1 and A_2 are the amplitudes of the components. τ_1 and τ_2 are decay times. f_1 and f_2 are fractional contributions. $f_i = \frac{A_i\tau_i}{\sum_{i=1}^{n} A_i\tau_i}$, where n is the number of decay channels.

red (720 nm) emission bands have fast and slow decay components. However, the fast decay component dominates the dynamics of the blue emission band, contributing ~89% to the total emission. The slow decay component dominates the red emission band, contributing ~98% to the total emission. Different lifetimes reveal different emission states. These results demonstrate that the band-edge states emit light two orders of magnitude faster than that of the midgap states.

The fast component (τ_1 = 1.84 ns) of the red emission is close to that in the blue emission (τ_1 = 1.27 ns), indicating a fast charge trapping from the band-edge state to the midgap state. However, the fast component contributes only 2% of the total red emission. The trapping process is likely inefficient, which explains the negligible red emission from the CdS nanoribbons when they are excited at 337 nm (above the bandgap) (Figure 2b).

The blue emission has a slow decay component (τ_2 = 256 ns), which is close to the slow decay component in the red emission (τ_2 = 268 ns). The slow decay may be due to the recombination of the exciton after a temporary charge separation, as demonstrated in CdSe nanoplatelets by Rabouw et al.[39] It could also come from the band-edge emission via the shallow surface trap states, which was proposed to explain the slow band-edge emission in CdS quantum dots.[45]

The light-emitting states are further studied using cathodoluminescence spectroscopy. The cathodoluminescence was collected from a film of CdS nanoribbons mounted inside an electron microscope (section H of the Supporting Information). In contrast to photoluminescence whose intensity is proportional to the absorption cross section of the states, cathodoluminescence is less selective. All of the available states can be excited.[46] We fabricated the sample by drop-casting the nanoribbons onto a glass substrate. The nanoribbon film was first studied using optical spectroscopy. When the nanoribbon film is excited with an ultraviolet laser, its photoluminescence spectrum is nearly the same as that of the nanoribbons in solution (section I of the Supporting Information). It also shows a red emission when it is under a sub-bandgap excitation. These results show the transition from the solution to the solid does not affect the light-emitting states in CdS nanoribbons.

The scanning electron microscopy (SEM) image of the film (Figure 5a) shows clustered CdS nanoribbons that are similar

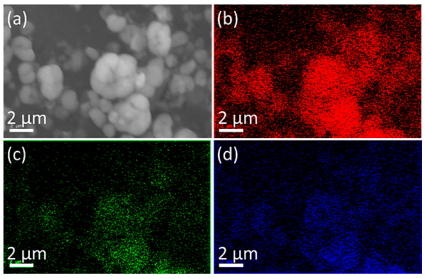

Figure 5. (a) SEM image of the colloidal CdS nanoribbons. (b−d) Red, green, and blue cathodoluminescence images, respectively, of the same nanoribbons.

to those in the TEM images at a low resolution (section C of the Supporting Information). The cathodoluminescence from the nanoribbons (Figure 5b−d) shows the same profile as the SEM image (Figure 5a). This proves that the cathodoluminescence comes from the nanoribbons. The cathodoluminescence shows all of the blue, green, and red emissions (Figure 5b−d).

The intensity of cathodoluminescence has a red:green:blue ratio of 15:4:8. The red cathodoluminescence from the nanoribbon is stronger than the blue and green ones. This indicates the red emission from CdS nanoribbons is efficient. It can be exploited for red-light-emitting diodes, as demonstrated with CdS quantum dots.[47] Our photoluminescence study shows the process of charge trapping into the midgap states is not efficient. Therefore, it is possible to excite the electron into different states to emit light of different colors in the visible spectrum. Using both CdS and PbS nanoribbons,[25] we can expand the emission spectrum between 400 and 2000 nm.

In conclusion, we demonstrate a full conversion of colloidal PbS nanoribbons into CdS nanoribbons via cation exchange. This method preserves the size and shape of nanoribbons but changes the crystal structure from rock salt to zincblende. The basal plane of the nanoribbon also changes from the (100) to (111) plane. The corresponding emission spectrum shifts from

https://doi.org/10.1021/acs.jpclett.2c02390
J. Phys. Chem. Lett. 2022, 13, 8987−8992

infrared to visible. The blue band-edge emission from CdS nanoribbons is fast, while the red midgap emission is slow. The cathodoluminescence from the CdS nanoribbons shows the presence of red, green, and blue emission bands. These emission states can be used for multicolor light-emitting diodes or bioimaging. Using colloidal CdS and PbS nanoribbons, we can fabricate light-emitting devices with a spectrum spanning from visible to infrared.

■ ASSOCIATED CONTENT

Supporting Information

The Supporting Information is available free of charge at https://pubs.acs.org/doi/10.1021/acs.jpclett.2c02390.

Synthesis of PbS nanoribbons, cation-exchange reaction, energy-dispersive X-ray spectroscopy, X-ray diffraction of quantum dots, annealing treatment, annealing effect, lifetime measurements, cathodoluminescence, and optical spectroscopy of the CdS nanoribbon film (PDF)

■ AUTHOR INFORMATION

Corresponding Author

Liangfeng Sun − *Department of Physics and Astronomy and Center for Photochemical Sciences, Bowling Green State University, Bowling Green, Ohio 43403, United States;* orcid.org/0000-0003-0527-1777; Email: lsun@bgsu.edu

Authors

Zhoufeng Jiang − *Department of Physics and Astronomy and Center for Photochemical Sciences, Bowling Green State University, Bowling Green, Ohio 43403, United States*

Yiteng Tang − *Department of Physics and Astronomy and Center for Photochemical Sciences, Bowling Green State University, Bowling Green, Ohio 43403, United States;* orcid.org/0000-0002-7533-756X

Antara Debnath Antu − *Department of Physics and Astronomy, Bowling Green State University, Bowling Green, Ohio 43403, United States*

Shashini M. Premathilaka − *Department of Physics and Astronomy and Center for Photochemical Sciences, Bowling Green State University, Bowling Green, Ohio 43403, United States*

Marilyn Louise Cayer − *Department of Biological Sciences, Bowling Green State University, Bowling Green, Ohio 43403, United States*

Carol A. Heckman − *Department of Biological Sciences, Bowling Green State University, Bowling Green, Ohio 43403, United States*

Pavel Moroz − *Department of Physics and Astronomy and Center for Photochemical Sciences, Bowling Green State University, Bowling Green, Ohio 43403, United States*

Mikhail Zamkov − *Department of Physics and Astronomy and Center for Photochemical Sciences, Bowling Green State University, Bowling Green, Ohio 43403, United States;* orcid.org/0000-0002-8638-2972

Complete contact information is available at: https://pubs.acs.org/10.1021/acs.jpclett.2c02390

Author Contributions

‖Z.J. and Y.T. contributed equally to this work.

Notes

The authors declare no competing financial interest.

■ ACKNOWLEDGMENTS

This material is based upon work supported by the National Science Foundation under Grant 1905217. The work is partially supported with funding provided by the Office of the Vice President for Research & Economic Development, Bowling Green State University. L.S. is thankful for the funding provided by the U.S. Air Force Research Lab Summer Faculty Fellowship Program. The authors thank Charles Codding (machine shop) and Doug Martin (electronic shop) for their technical assistance at Bowling Green State University. The authors thank Joseph G. Lawrence for his help on the TEM measurements at the University of Toledo. P.M. and M.Z. were supported by Grant DE-SC0016872 (M.Z.) funded by the U.S. Department of Energy, Office of Science.

■ REFERENCES

(1) Liu, Y.; Wayman, V. L.; Gibbons, P. C.; Loomis, R. A.; Buhro, W. E. Origin of High Photoluminescence Efficiencies in CdSe Quantum Belts. *Nano Lett.* **2010**, *10*, 352−357.

(2) Liu, Y.; Wang, F.; Wang, Y.; Gibbons, P. C.; Buhro, W. E. Lamellar Assembly of Cadmium Selenide Nanoclusters into Quantum Belts. *J. Am. Chem. Soc.* **2011**, *133*, 17005−17013.

(3) Li, Z.; Peng, X. Size/Shape-Controlled Synthesis of Colloidal CdSe Quantum Disks: Ligand and Temperature Effects. *J. Am. Chem. Soc.* **2011**, *133*, 6578−6586.

(4) Li, Z.; Qin, H.; Guzun, D.; Benamara, M.; Salamo, G.; Peng, X. Uniform Thickness and Colloidal-Stable CdS Quantum Disks with Tunable Thickness: Synthesis and Properties. *Nano Research* **2012**, *5*, 337−351.

(5) Ithurria, S.; Dubertret, B. Quasi 2D Colloidal CdSe Platelets with Thicknesses Controlled at the Atomic Level. *J. Am. Chem. Soc.* **2008**, *130*, 16504−16505.

(6) Ma, X.; Diroll, B. T.; Cho, W.; Fedin, I.; Schaller, R. D.; Talapin, D. V.; Gray, S. K.; Wiederrecht, G. P.; Gosztola, D. J. Size-Dependent Biexciton Quantum Yields and Carrier Dynamics of Quasi-Two-Dimensional Core/Shell Nanoplatelets. *ACS Nano* **2017**, *11*, 9119−9127.

(7) Tessier, M. D.; Mahler, B.; Nadal, B.; Heuclin, H.; Pedetti, S.; Dubertret, B. Spectroscopy of Colloidal Semiconductor Core/Shell Nanoplatelets with High Quantum Yield. *Nano Lett.* **2013**, *13*, 3321−3328.

(8) Ithurria, S.; Tessier, M. D.; Mahler, B.; Lobo, R. P. S. M.; Dubertret, B.; Efros, A. L. Colloidal Nanoplatelets with Two-Dimensional Electronic Structure. *Nat. Mater.* **2011**, *10*, 936−941.

(9) She, C.; Fedin, I.; Dolzhnikov, D. S.; Demortière, A.; Schaller, R. D.; Pelton, M.; Talapin, D. V. Low-Threshold Stimulated Emission using Colloidal Quantum Wells. *Nano Lett.* **2014**, *14*, 2772−2777.

(10) Yang, Z.; Pelton, M.; Fedin, I.; Talapin, D. V.; Waks, E. A Room Temperature Continuous-Wave Nanolaser using Colloidal Quantum Wells. *Nat. Commun.* **2017**, *8*, 143.

(11) Grim, J. Q.; Christodoulou, S.; Di Stasio, F.; Krahne, R.; Cingolani, R.; Manna, L.; Moreels, I. Continuous-Wave Biexciton Lasing at Room Temperature using Solution-Processed Quantum Wells. *Nat. Nanotechnol.* **2014**, *9*, 891.

(12) She, C.; Fedin, I.; Dolzhnikov, D. S.; Dahlberg, P. D.; Engel, G. S.; Schaller, R. D.; Talapin, D. V. Red, Yellow, Green, and Blue Amplified Spontaneous Emission and Lasing using Colloidal CdSe Nanoplatelets. *ACS Nano* **2015**, *9*, 9475−9485.

(13) Li, M.; Zhi, M.; Zhu, H.; Wu, W.; Xu, Q.; Jhon, M. H.; Chan, Y. Ultralow-Threshold Multiphoton-Pumped Lasing from Colloidal Nanoplatelets in Solution. *Nat. Commun.* **2015**, *6*, 8513.

(14) Guzelturk, B.; Kelestemur, Y.; Olutas, M.; Delikanli, S.; Demir, H. V. Amplified Spontaneous Emission and Lasing in Colloidal Nanoplatelets. *ACS Nano* **2014**, *8*, 6599−6605.

(15) Jiang, Z.; Bhandari, G. B.; Premathilaka, S. M.; Khan, S.; Dimick, D. M.; Stombaugh, C.; Mandell, A.; He, Y.; Peter Lu, H.; Sun, L. Growth of Colloidal PbS Nanosheets and the Enhancement of

their Photoluminescence. *Phys. Chem. Chem. Phys.* **2015**, *17*, 23303−23307.
(16) Zhang, H.; Savitzky, B. H.; Yang, J.; Newman, J. T.; Perez, K. A.; Hyun, B.; Kourkoutis, L. F.; Hanrath, T.; Wise, F. W. Colloidal Synthesis of PbS and PbS/CdS Nanosheets using Acetate-Free Precursors. *Chem. Mater.* **2016**, *28*, 127−134.
(17) Schliehe, C.; Juarez, B. H.; Pelletier, M.; Jander, S.; Greshnykh, D.; Nagel, M.; Meyer, A.; Foerster, S.; Kornowski, A.; Klinke, C.; et al. Ultrathin PbS Sheets by Two-Dimensional Oriented Attachment. *Science* **2010**, *329*, 550−553.
(18) Bielewicz, T.; Ramin Moayed, M. M.; Lebedeva, V.; Strelow, C.; Rieckmann, A.; Klinke, C. From Dots to Stripes to Sheets: Shape Control of Lead Sulfide Nanostructures. *Chem. Mater.* **2015**, *27*, 8248−8254.
(19) Premathilaka, S. M.; Jiang, Z.; Antu, A.; Leffler, J.; Hu, J.; Roy, A.; Sun, L. A Robust Method for the Synthesis of Colloidal PbS Nanosheets. *Phys. Status Solidi RRL* **2016**, *10*, 838−842.
(20) Antu, A. D.; Jiang, Z.; Premathilka, S. M.; Tang, Y.; Hu, J.; Roy, A.; Sun, L. Bright Colloidal PbS Nanoribbons. *Chem. Mater.* **2018**, *30*, 3697−3703.
(21) Aerts, M.; Bielewicz, T.; Klinke, C.; Grozema, F. C.; Houtepen, A. J.; Schins, J. M.; Siebbeles, L. D. A. Highly Efficient Carrier Multiplication in PbS Nanosheets. *Nat. Commun.* **2014**, *5*, 3789.
(22) Dogan, S.; Bielewicz, T.; Lebedeva, V.; Klinke, C. Photovoltaic Effect in Individual Asymmetrically Contacted Lead Sulfide Nanosheets. *Nanoscale* **2015**, *7*, 4875−4883.
(23) Dogan, S.; Bielewicz, T.; Cai, Y.; Klinke, C. Field−effect Transistors made of Individual Colloidal PbS Nanosheets. *Appl. Phys. Lett.* **2012**, *101*, 073102.
(24) Wan, W.; Yao, Y.; Sun, L.; Liu, C.; Zhang, F. Topological, Valleytronic, and Optical Properties of Monolayer PbS. *Adv. Mater.* **2017**, *29*, 1604788.
(25) Bhandari, G. B.; Subedi, K.; He, Y.; Jiang, Z.; Leopold, M.; Reilly, N.; Lu, H. P.; Zayak, A. T.; Sun, L. Thickness-Controlled Synthesis of Colloidal PbS Nanosheets and their Thickness-Dependent Energy Gaps. *Chem. Mater.* **2014**, *26*, 5433−5436.
(26) Khan, A. H.; Brescia, R.; Polovitsyn, A.; Angeloni, I.; Martín-García, B.; Moreels, I. Near-Infrared Emitting Colloidal PbS Nanoplatelets: Lateral Size Control and Optical Spectroscopy. *Chem. Mater.* **2017**, *29*, 2883−2889.
(27) Premathilaka, S. M.; Tang, Y.; Jiang, Z.; MDS Weeraddana, T.; Debnath Antu, A.; Bischoff, S.; Sun, L. Controlling the Lateral Size and Excitonic Properties of Colloidal PbS Nanosheets. *ChemNanoMat* **2020**, *6*, 816−820.
(28) Son, D. H.; Hughes, S. M.; Yin, Y.; Paul Alivisatos, A. Cation Exchange Reactions in Ionic Nanocrystals. *Science* **2004**, *306*, 1009−1012.
(29) Robinson, R. D.; Sadtler, B.; Demchenko, D. O.; Erdonmez, C. K.; Wang, L.; Alivisatos, A. P. Spontaneous Superlattice Formation in Nanorods through Partial Cation Exchange. *Science* **2007**, *317*, 355−358.
(30) Pietryga, J. M.; Werder, D. J.; Williams, D. J.; Casson, J. L.; Schaller, R. D.; Klimov, V. I.; Hollingsworth, J. A. Utilizing the Lability of Lead Selenide to Produce Heterostructured Nanocrystals with Bright, Stable Infrared Emission. *J. Am. Chem. Soc.* **2008**, *130*, 4879−4885.
(31) De Trizio, L.; Manna, L. Forging Colloidal Nanostructures Via Cation Exchange Reactions. *Chem. Rev.* **2016**, *116*, 10852−10887.
(32) Justo, Y.; Sagar, L. K.; Flamee, S.; Zhao, Q.; Vantomme, A.; Hens, Z. Less is More. Cation Exchange and the Chemistry of the Nanocrystal Surface. *ACS Nano* **2014**, *8*, 7948−7957.
(33) Khan, S.; Jiang, Z.; Premathilka, S. M.; Antu, A.; Hu, J.; Voevodin, A. A.; Roland, P. J.; Ellingson, R. J.; Sun, L. Few-Atom-Thick Colloidal PbS/CdS Core/Shell Nanosheets. *Chem. Mater.* **2016**, *28*, 5342−5346.
(34) Lechner, R. T.; Fritz-Popovski, G.; Yarema, M.; Heiss, W.; Hoell, A.; Schülli, T. U.; Primetzhofer, D.; Eibelhuber, M.; Paris, O. Crystal Phase Transitions in the Shell of PbS/CdS Core/Shell Nanocrystals Influences Photoluminescence Intensity. *Chem. Mater.* **2014**, *26*, 5914−5922.
(35) Zhukovskyi, M.; Tongying, P.; Yashan, H.; Wang, Y.; Kuno, M. Efficient Photocatalytic Hydrogen Generation from Ni Nanoparticle Decorated CdS Nanosheets. *ACS Catal.* **2015**, *5*, 6615−6623.
(36) Jain, P. K.; Beberwyck, B. J.; Fong, L.; Polking, M. J.; Alivisatos, A. P. Highly Luminescent Nanocrystals from Removal of Impurity Atoms Residual from Ion-Exchange Synthesis. *Angew. Chem., Int. Ed.* **2012**, *51*, 2387−2390.
(37) Diroll, B. T.; Talapin, D. V.; Schaller, R. D. Violet-to-Blue Gain and Lasing from Colloidal CdS Nanoplatelets: Low-Threshold Stimulated Emission Despite Low Photoluminescence Quantum Yield. *ACS Photonics* **2017**, *4*, 576−583.
(38) Clark, S. W.; Harbold, J. M.; Wise, F. W. Resonant Energy Transfer in PbS Quantum Dots. *J. Phys. Chem. C* **2007**, *111*, 7302−7305.
(39) Rabouw, F. T.; van der Bok, J. C.; Spinicelli, P.; Mahler, B.; Nasilowski, M.; Pedetti, S.; Dubertret, B.; Vanmaekelbergh, D. Temporary Charge Carrier Separation Dominates the Photoluminescence Decay Dynamics of Colloidal CdSe Nanoplatelets. *Nano Lett.* **2016**, *16*, 2047−2053.
(40) Naeem, A.; Masia, F.; Christodoulou, S.; Moreels, I.; Borri, P.; Langbein, W. Giant Exciton Oscillator Strength and Radiatively Limited Dephasing in Two-Dimensional Platelets. *Phys. Rev. B* **2015**, *91*, 121302.
(41) Ramsden, J. J.; Webber, S. E.; Graetzel, M. Luminescence of Colloidal Cadmium Sulfide Particles in Acetonitrile and Acetonitrile/Water Mixtures. *J. Phys. Chem.* **1985**, *89*, 2740−2743.
(42) Vuylsteke, A. A.; Sihvonen, Y. T. Sulfur Vacancy Mechanism in Pure CdS. *Phys. Rev.* **1959**, *113*, 40−42.
(43) Wei, H. H.; Evans, C. M.; Swartz, B. D.; Neukirch, A. J.; Young, J.; Prezhdo, O. V.; Krauss, T. D. Colloidal Semiconductor Quantum Dots with Tunable Surface Composition. *Nano Lett.* **2012**, *12*, 4465−4471.
(44) Anderson, N. C.; Hendricks, M. P.; Choi, J. J.; Owen, J. S. Ligand Exchange and the Stoichiometry of Metal Chalcogenide Nanocrystals: Spectroscopic Observation of Facile Metal-Carboxylate Displacement and Binding. *J. Am. Chem. Soc.* **2013**, *135*, 18536−18548.
(45) Veamatahau, A.; Jiang, B.; Seifert, T.; Makuta, S.; Latham, K.; Kanehara, M.; Teranishi, T.; Tachibana, Y. Origin of Surface Trap States in CdS Quantum Dots: Relationship between Size Dependent Photoluminescence and Sulfur Vacancy Trap States. *Phys. Chem. Chem. Phys.* **2015**, *17*, 2850−2858.
(46) Robins, L. H.; Cook, L. P.; Farabaugh, E. N.; Feldman, A. Cathodoluminescence of Defects in Diamond Films and Particles Grown by Hot-Filament Chemical-Vapor Deposition. *Phys. Rev. B* **1989**, *39*, 13367−13377.
(47) Bansal, A. K.; Antolini, F.; Zhang, S.; Stroea, L.; Ortolani, L.; Lanzi, M.; Serra, E.; Allard, S.; Scherf, U.; Samuel, I. D. W. Highly Luminescent Colloidal CdS Quantum Dots with Efficient Near-Infrared Electroluminescence in Light-Emitting Diodes. *J. Phys. Chem. C* **2016**, *120*, 1871−1880.

https://doi.org/10.1021/acs.jpclett.2c02390
J. Phys. Chem. Lett. 2022, 13, 8987−8992